Theoretical study and optimization of a high power mid-infrared erbium-doped ZBLAN fibre laser*

Li Jian-Feng(李剑峰)[a)†] and Stuart D. Jackson[b)]

[a)] *School of Optoelectronic Information, University of Electronic Science and Technology of China, Chengdu* 610054, *China*

[b)] *Institute of Photonics and Optical Science, School of Physics, University of Sydney, Camperdown* 2006, *Australia*

(Received 28 September 2010; revised manuscript received 14 October 2010)

Based on the rate equations describing the erbium-doped fluoride glass (ZBLAN) fibre lasers with different pumping configurations being taken into account, this paper presents theoretical calculations related to the dynamic population density and the operation performance of a high power mid-infrared all-fibre erbium-doped ZBLAN fibre laser. It shows that the ground-state absorption, excited-state absorption and energy-transfer-upconversion processes co-exist and produce a population balance, causing the laser to operate stably at a continuous wave state. A good agreement between the theoretical results and recent experimental measurement is obtained. Furthermore, the laser structure parameters including fibre length, reflectance of output fibre Bragg grating and pumping configurations are quantitatively optimised to achieve the best performance. The results show, as expected, that the slope efficiency of the fibre laser can be improved significantly through optimisation, which then provides an important guide for the design of high-performance mid-infrared erbium-doped ZBLAN fibre lasers.

Keywords: erbium-doped fibre laser, mid-infrared fibre laser, ZBLAN fibre, rate equations
PACS: 42.55.Wd, 42.55.Xi, 42.60.Lh **DOI:** 10.1088/1674-1056/20/3/034205

1. Introduction

There is a strong interest in the development of mid-infrared (IR) fibre lasers mainly because of their potential applications in laser surgery,[1,2] frequency conversion[3] and spectroscopy.[4] High-quality cutting or ablation of biological tissues using erbium-doped solid state lasers has been demonstrated.[5] Erbium-doped fluoride glass (ZBLAN) fibre lasers have many advantages over bulk solid-state lasers, including better beam quality, higher conversion efficiency and excellent heat dissipation, and thus are promising candidates for the construction of compact and efficient laser sources, which can provide large flexibility and high laser intensity for surgical applications. A number of demonstrations of high power ~ 3 μm fibre lasers based on fluoride glass fibres using active ions such as erbium,[6,7] holmium[8,9] and dysprosium[10] have been reported.

The lack of commercial high power pump diodes which emit at the 1100 nm and 1300 nm required for pumping holmium and dysprosium doped ZBLAN fibre lasers, respectively, has limited the achievable output power. For the 790 nm and 975 nm absorption bands of erbium, high power diodes are readily available. Therefore, erbium-doped ZBLAN fibre lasers are currently the most practical and convenient high power ~ 3 μm lasers. Even though the Stokes-efficiency limits at 790 nm and 975 nm pumping are lower than that at 1100 nm and 1300 nm pumping. There has been significant progress in the erbium-doped ZBLAN fibre lasers lately, thanks to the increasing availability of high-quality erbium-doped ZBLAN fibres. In the year 1999, Jackson *et al.* reported the first mid-IR fibre laser with 1.7 W output power and 17.3% slope efficiency at 2.71 μm from a double-clad erbium-doped ZBLAN fibre diode pumped at 790 nm.[11] Based on the same idea, Zhu and Jain demonstrated an erbium-doped ZBLAN fibre laser with 9 W output power at 2.78 μm diode pumped at 975 nm.[12] Recently, Faucher *et al.* reported the first all-fibre erbium-doped ZBLAN fibre laser with 5.2 W output power at 2.94 μm diode pumped at 975 nm,[13] which indicates that the practical application of mid-IR fibre laser will come true in the near future. Pollnau and Jackson constructed

*Project supported by the China Postdoctoral Science Foundation (Grant No. 20090451417), the China Postdoctoral Science Special Foundation (Grant No. 201003693), the Fundamental Research Funds for the Central Universities of China (Grant No. ZYGX2009J053) and the National Natural Science Foundation of China (Grant No. 60736038).

†Corresponding author. E-mail: lijianfeng@uestc.edu.cn

© 2011 Chinese Physical Society and IOP Publishing Ltd

the theoretical model of the erbium 3 μm fibre laser and investigated the fundamental physics in detail, e.g., ground-state absorption (GSA), excited-state absorption (ESA), energy-transfer upconversion (ETU), cascade lasing.[14] The energy recycling by ETU from the lower to the upper laser level can increase the slope efficiency to values greater than the Stokes efficiency, which is similar to a number of Er^{3+}-doped crystal lasers. The transition rate for this ETU process increases as the Er^{3+} concentration increases and hence the performance of erbium-doped ZBLAN fibre lasers is theoretically better at higher Er^{3+} concentrations.[15] Although the fundamental mechanism of erbium 3 μm fibre lasers are well understood, there has been no relevant quantitative analysis and optimisation concerning the structure of erbium-doped ZBLAN fibre lasers including fibre length, reflectance of output coupler and pumping configurations, which are very important to enable the lasers to achieve the best performance.

In this paper, we investigate theoretically the population density dynamic characteristics and continuous wave (CW) operation performance for high power mid-infrared erbium-doped ZBLAN double-clad fibre lasers according to a rate equation model. Using the measured ETU and cross relaxation (CR) parameters relevant to erbium-doped ZBLAN fibre, we obtain a good agreement between the theoretical results and recent experimental data in Ref. [13]. Furthermore, the laser structure parameters, including fibre length, reflectance of output coupler and pumping configurations are quantitatively analysed and optimised for the best performance. The results show that the fibre length and output reflectance of output coupler strongly affect the output power, while the effects of different pumping configurations including forward, backward and two-end pumping on laser performance can be ignored. It is shown that the slope efficiency of the fibre laser can be increased vastly through optimisation.

2. Rate-equation model

Figure 1 shows the energy-level scheme for the erbium-doped 3 μm ZBLAN fibre laser. It is seen that the GSA of pump-laser radiation at 975 nm excites the Er^{3+} ions to the $^4I_{11/2}$ level. The ESA at 975 nm excites the Er^{3+} ions from the $^4I_{11/2}$ level to the $^4F_{7/2}$ level, which is detrimental to lasing and must be avoided. Fortunately, the ESA is much less important in the double-clad ZBLAN fibre because the reduced pump intensity leads to smaller excitation densities. The relevant laser transition occurs between the $^4I_{11/2}$ and the $^4I_{13/2}$ levels in the ZBLAN glass. The ETU_1 process ($^4I_{13/2}$, $^4I_{13/2}$)→($^4I_{15/2}$, $^4I_{9/2}$) leads to a fast depletion of the lower laser level, which enables the CW operation of laser transition.[14] Otherwise, the laser transition will be self-terming due to the long lower-level lifetime of 9.0 ms. Half of the ions are upconverted to the $^4I_{9/2}$ level by ETU_1 and are recycled to the $^4I_{11/2}$ upper laser level by subsequent multiphonon relaxation, from which they can each emit a second laser photon. This process can increase the quantum efficiency $\eta_q = \eta_l/\eta_p$ of pump photons η_p converted to laser photons η_l and provide the potentiality for obtaining high output power.[16] The population density in the $^4I_{11/2}$ upper laser level may be decreased by ETU_2 process ($^4I_{11/2}$, $^4I_{11/2}$)→($^4F_{7/2}$, $^4I_{15/2}$), resulting in the reduction of slope efficiency.

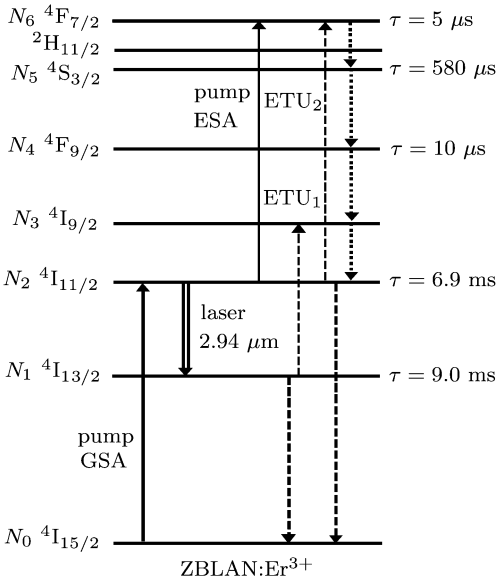


Fig. 1. Schematic diagram of erbium-doped ZBLAN fibre showing the GSA, the ESA, the ETU and the CR.

A schematic diagram of the layout of a typical all-fibre double-clad erbium-doped ZBLAN fibre laser is shown in Fig. 2. The light from the diode pump laser at 976 nm is coupled into the inner cladding of the double-clad fibre by the butt coupling method. The high-reflector (HR) and the low-reflector (LR) fibre Bragg gratings (FBGs) are written in the double-clad ZBLAN fibre by using high energy femtosecond pulses, constructing the Fabry-Perot cavity.

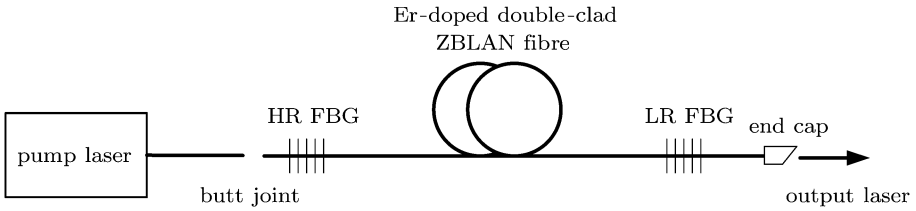


Fig. 2. Schematic demonstration of an all-fibre double-clad erbium-doped ZBLAN fibre laser.

To quantitatively understand the behaviour of the erbium-doped ZBLAN fibre laser and to explore potential ways of power scaling, the laser system is investigated theoretically using rate equations. We have modified the equation describing the operation of the erbium-doped ZBLAN fibre laser in Ref. [15] to take into account different pumping configurations. The local absorption coefficient within the longitudinal spatial element of width $\Delta l(z)$ is given by

$$\alpha(z) = \sigma_{\rm GSA} N_0(z) + \sigma_{\rm ESA} N_2(z), \tag{1}$$

where N_i are the local population densities, $\sigma_{\rm GSA}$ and $\sigma_{\rm ESA}$ represent the cross-sections for $^4{\rm I}_{15/2} \rightarrow {}^4{\rm I}_{11/2}$ ground-state absorption (GSA) and $^4{\rm I}_{11/2} \rightarrow {}^4{\rm F}_{7/2}$ ESA processes, respectively. The effective absorption coefficient of the fibre is given by

$$\alpha_{\rm eff}(z) = \alpha(z)\pi r_{\rm core}^2 / A_{\rm clad}, \tag{2}$$

where $r_{\rm core}$ and $A_{\rm clad}$ are the core radius and the cladding area, respectively. The launched pump power into an individual longitudinal spatial element for the forward, backward and two end pumping configurations, respectively, are calculated from

$$P_{\rm fl}(z) = \eta_{\rm fin} P_{\rm fin} \prod_{z'=1}^{z-1} \{\exp[-\Delta l(z')\alpha_{\rm eff}(z')]\}, \tag{3}$$

$$P_{\rm bl}(z) = \eta_{\rm bin} P_{\rm bin} \prod_{z'=n-1}^{z} \{\exp[-\Delta l(z')\alpha_{\rm eff}(z')]\}, \tag{4}$$

$$P_{\rm twol}(z) = P_{\rm fl}(z) + P_{\rm bl}(z), \tag{5}$$

where $P_{\rm fin}$ and $P_{\rm bin}$ are the incident pump powers for the forward and backward pumping, respectively. The $\eta_{\rm fin}$ and $\eta_{\rm bin}$ are the launch efficiency coefficients for the forward and backward pumping, respectively. With Eqs. (1)–(5), the equations for the local GSA and ESA pump rates are

$$\begin{aligned} R_{\rm GSA/ESA}(z) = {} & [\sigma_{\rm GSA/ESA} N_{0/2}(z)/\alpha(z)] \\ & \times \{1 - \exp[-\Delta l(z)\alpha_{\rm eff}(z)]\} \\ & \times \lambda_{\rm p}/(hc\Delta l \pi r_{\rm core}^2) P_{\rm l}(z), \end{aligned} \tag{6}$$

where h and c denote the Planck's constant and the speed of light in vacuum, respectively. According to the rate equation model shown in Fig. 1, the rate equations for the population densities $N_i(z)$ are given by

$$\frac{{\rm d}N_6(z)}{{\rm d}t} = R_{\rm ESA}(z) - \tau_6^{-1} N_6(z) + W_{22} N_2^2(z), \tag{7}$$

$$\begin{aligned} \frac{{\rm d}N_5(z)}{{\rm d}t} = {} & \beta_{65}\tau_6^{-1} N_6(z) - \tau_5^{-1} N_5(z) \\ & - W_{50} N_5(z) N_0(z), \end{aligned} \tag{8}$$

$$\frac{{\rm d}N_4(z)}{{\rm d}t} = \sum_{i=5,6} \left[\beta_{i4}\tau_i^{-1} N_i(z)\right] - \tau_4^{-1} N_4(z), \tag{9}$$

$$\begin{aligned} \frac{{\rm d}N_3(z)}{{\rm d}t} = {} & \sum_{i=4,\ldots,6} \left[\beta_{i3}\tau_i^{-1} N_i(z)\right] - \tau_3^{-1} N_3(z) \\ & + W_{50} N_5(z) N_0(z) + W_{11} N_1^2(z), \end{aligned} \tag{10}$$

$$\begin{aligned} \frac{{\rm d}N_2(z)}{{\rm d}t} = {} & R_{\rm GSA}(z) - R_{\rm ESA}(z) \\ & + \sum_{i=3,\ldots,6} \left[\beta_{i2}\tau_i^{-1} N_i(z)\right] - \tau_2^{-1} N_2(z) \\ & - 2W_{22} N_2^2(z) - R_{\rm SE}(z), \end{aligned} \tag{11}$$

$$\begin{aligned} \frac{{\rm d}N_1(z)}{{\rm d}t} = {} & \sum_{i=2,\ldots,6} \left[\beta_{i1}\tau_i^{-1} N_i(z)\right] - \tau_1^{-1} N_1(z) \\ & + W_{50} N_5(z) N_0(z) - 2W_{11} N_1^2(z) \\ & + R_{\rm SE}(z), \end{aligned} \tag{12}$$

$$N_{\rm Er} = \sum_{i=0,\ldots,6} N_i, \tag{13}$$

where τ_i represents the intrinsic lifetimes of the system at low dopant concentration and takes into accont radiative as well as multiphonon relaxation. The β_{ij} represents the branching ration for decay from level i into lower level j. The values of τ_i and β_{ij} can be found in Ref. [15]. The W_{11} and W_{22} represent the ETU parameters for ETU from the $^4{\rm I}_{13/2}$ and $^4I_{11/2}$ energy levels, respectively. The W_{50} represents the CR parameter from the thermally coupled $^4{\rm S}_{3/2}$, $^2{\rm H}_{11/2}$ energy levels. The rate equation of the photon density ϕ for the laser transition between the $^4{\rm I}_{11/2}$ level and the $^4{\rm I}_{13/2}$ level (at 2.94 μm) is given by

$$\mathrm{d}\phi/\mathrm{d}t = (l/l_{\mathrm{opt}})\sum_{z=1}^{n} R_{\mathrm{SE}}(z) - \{-\ln(R_1R_2) + 2\kappa l\}\, c\phi/(2l_{\mathrm{opt}}), \quad (14)$$

where l_{opt} is the optical fibre length. The R_1 and R_2 are the reflectivities of the HR FBG and the LR FBG for the 2.94 μm emission, respectively. The stimulated-emission rates R_{SE} for the 2.94 μm emission is

$$R_{\mathrm{SE}}(z) = [b_2N_2(z) - (g_2/g_1)b_1N_1(z)]\,\sigma_{\mathrm{SE}}c\phi, \quad (15)$$

where the Boltzmann factors b_i (i = 1, 2) for $^4\mathrm{I}_{13/2}$ and $^4\mathrm{I}_{11/2}$ laser levels are taken from Ref. [17]. The Stark levels in Er^{3+} are Kramer degenerate, i.e., the degeneracies are $g_i = 2$. The σ_{SE} is the stimulated-emission cross-section for laser emission. The output power is given by

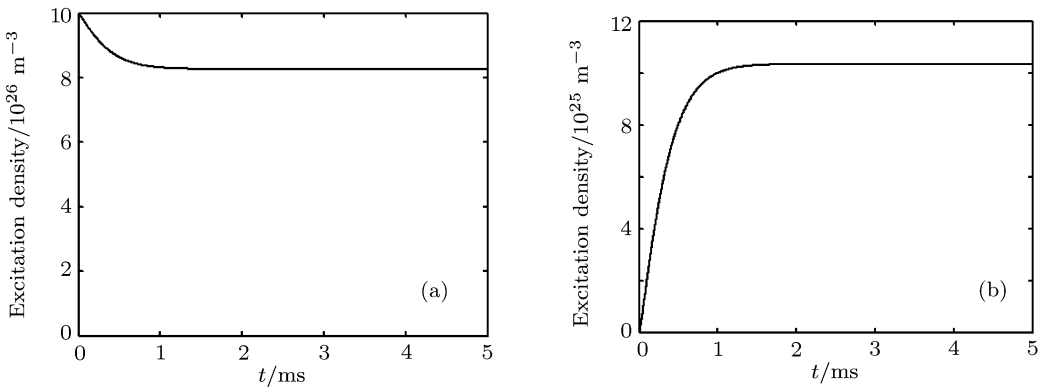
$$P_{\mathrm{out}} = c\phi(hc/\lambda_{21})\pi r_{\mathrm{core}}^2(1 - R_2). \quad (16)$$

The rate equations can be solved using a Runge–Kutta calculation of the fourth order with a longitudinal equal length discretization of the active medium of elements.

3. Results and discussions

In the simulation, the parameters used are the same as those in the experiment of Ref. [13]. The fibre specific parameters are: length l of 6.6 m, propagation loss κ of 400 dB/km. The D-shaped pump cladding is of 165×135 μm with a core diameter of 8 μm and a numerical aperture (NA) of 0.24. The GSA and the ESA cross-sections σ_{GSA} and σ_{ESA} are 2.1×10^{-21} cm^2 and 1.1×10^{-21} cm^2,[18] respectively. The measured overall pump absorption is $\sim$ 95% and the absorption coefficient can be calculated to be 0.454 dB/m. According to the equation $N_0 = \alpha_{\mathrm{eff}}A_{\mathrm{clad}}/\sigma_{\mathrm{GSA}}A_{\mathrm{core}}$ (without taking the effects of ESA into account), the Er^{3+} doping concentration N_{Er} can be approximately calculated to be 1.0×10^{21} cm^{-3}. According to Refs. [14] and [19], the ETU parameters W_{11} and W_{22} as well as the CR W_{50} for the concentration of 1.0×10^{21} cm^{-3} are estimated to be 2.8×10^{-17} cm^3·s^{-1}, 1×10^{-17} cm^3·s^{-1} and 2.7×10^{-17} cm^3·s^{-1}, respectively. The laser transition at 2.94 μm is assumed to originate in the lowest Stark level of $^4\mathrm{I}_{11/2}$ and terminate on the fifth Stark level of $^4\mathrm{I}_{13/2}$ with an emission cross-section σ_{21} of 5.7×10^{-21} cm^2. The reflection coefficients R_1 and R_2 for 2.94 μm radiation are assumed to be 90% and 15%, respectively. The simulation is performed with a longitudinal resolution of 8 finite elements which is sufficient for giving the effective absorption coefficient of 0.454 dB/m.

First, the dynamic characteristic of population density in each level is investigated. Figures 3(a)–3(g), respectively, show the variations of population densities $N_0 - N_6$ versus time t at the front end of fibre (the first longitudinal element of the simulation, where the pump absorption is the strongest) under the forward pump power of 10 W. The initial values of $N_0 - N_6$ are all set to be zero. It can be seen that $N_0 - N_6$ reach the steady state in about 2 ms, which shows that the fibre laser system can enter the stable state very quickly. The higher population densities in $^4\mathrm{I}_{13/2}$ and $^4\mathrm{I}_{11/2}$ levels than those in the other levels show that the GSA and laser transition are the dominant processes. In addition, the relative high population density N_3 in $^4\mathrm{I}_{9/2}$ level show that ETU_1 is also very strong, which can lead to a fast depletion of N_1 and recycle the energy. Owing to the fast quenching of ions in $^4\mathrm{F}_{9/2}$ and $^4\mathrm{F}_{7/2}$ levels resulting from their short lifetimes of 5 μs and 10 μs, respectively, the population densities N_6 and N_4 are very low.



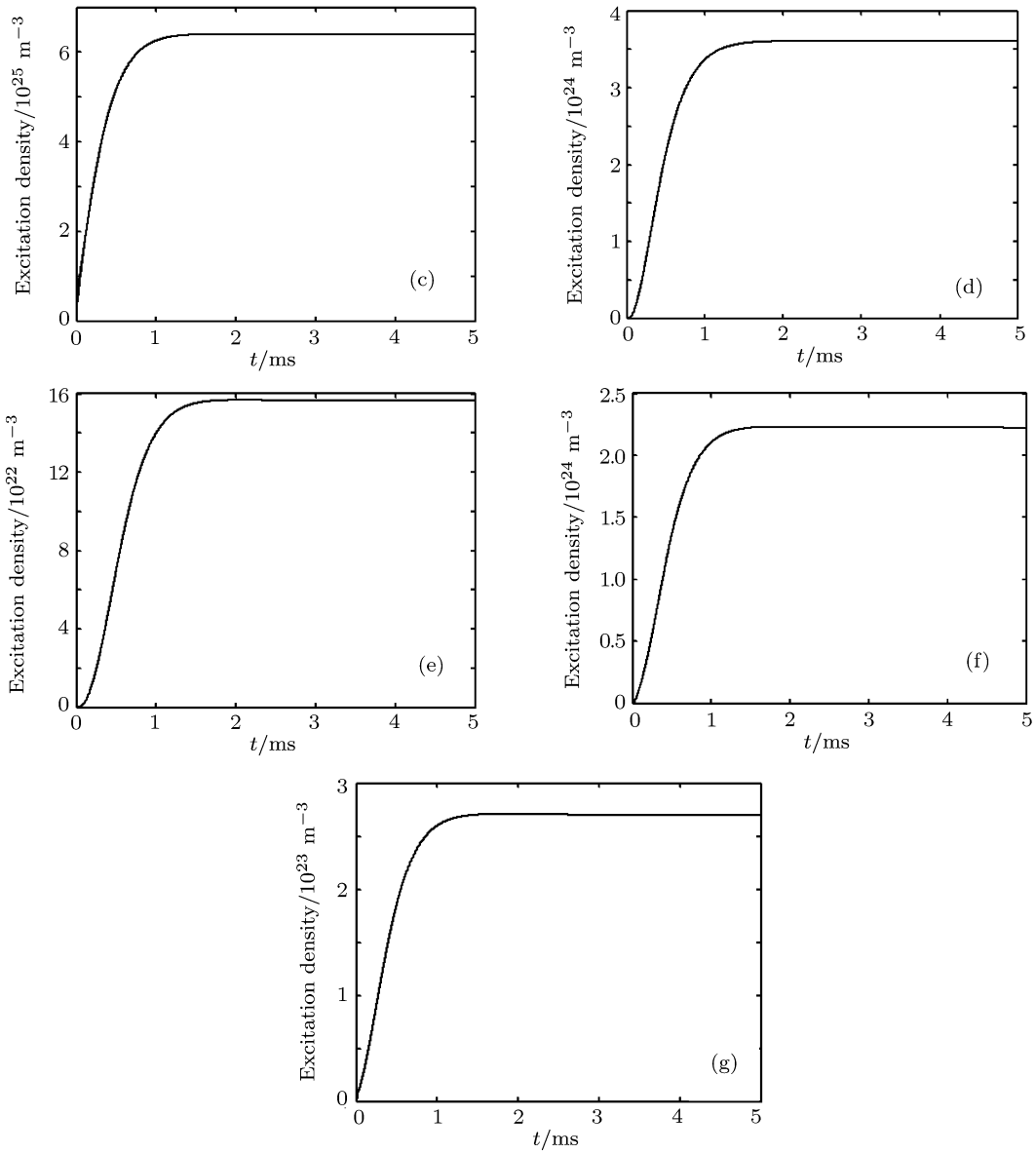


Fig. 3. Variation of $N_0 - N_6$ versus time t at fibre front end under forward pump power of 10 W. (a) N_0, (b) N_1, (c) N_2, (d) N_3, (e) N_4, (f) N_5, (g) N_6.

From the same simulation, the population densities N_0, N_1 and N_2 versus launched pump power are shown in Fig. 4. It can be seen that the population density N_0 decreases with the increasing launched pump power, as more ions are excited from the ground state to the $^4I_{11/2}$ level by the process of GSA under higher pump power. Meanwhile, the population density difference between the lasing Stark levels $^4I_{13/2}$ and $^4I_{11/2}$ increases with the increasing pump power, since the laser threshold inversion between the lasing Stark levels has to be maintained.

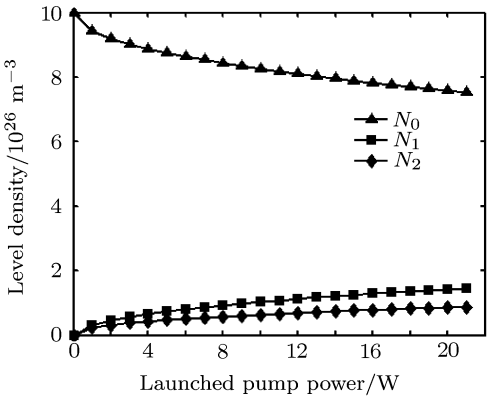


Fig. 4. Calculated population densities N_0, N_1 and N_2 versus launched pump power.

The output laser power calculated from the rate equations versus launched pump power is compared with the experimental data of the fibre laser in Ref. [13], as shown in Fig. 5. Good agreement of pump threshold and slope efficiency is obtained, which proves the validity of our theoretical model and the parameters used in the simulation.

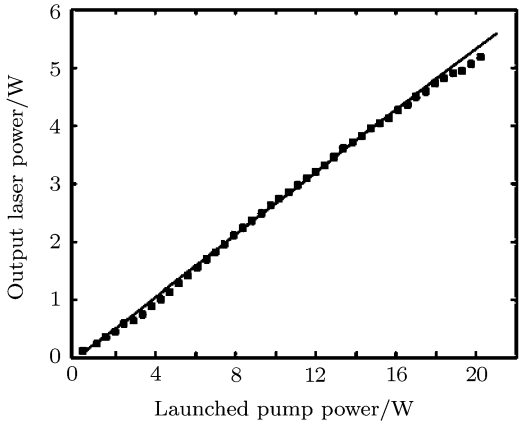


Fig. 5. Input-output characteristics of the all-fibre Er^{3+}-doped ZBLAN fibre laser. Experimental values (■) and calculated values (—).

Figure 6 shows the transition rates of GSA, ESA, surface-emitting (SE), ETU_1 and ETU_2 with the constant population densities versus the launched pump power at the fibre front end, where the other parameters are the same as those in Fig. 3. It can be seen that the transition rates of SE, GSA and ETU_1 continue to linearly and quickly increase with the launched pump power, and no saturation of the output power occurs. The rate of laser transition SE is the highest, GSA and ETU_1 have similar rates, which show that the laser operates at a stable state with a significantly reduced lifetime for the lower laser level due to ETU_1. In addition, ESA and ETU_2 have rates which are lower than 5% of SE rate due to the fast quenching of the population density in the $^4I_{11/2}$ upper laser level resulting from the high rate of laser transition ETU_1.

Due to the relative high fabrication cost of double-clad ZBLAN fibre and FBGs, it is necessary to theoretically optimise the laser system parameters, i.e., fibre length, reflectance of FBG and pumping configurations, to reduce the experimental number and obtain the best performance. Figure 7 shows the calculated output laser powers versus the fibre length for R_2 of 5%, 15% and 25%, respectively, for a launched pump power of 20 W. It can be seen that the output laser powers for different R_2 all increase first and then decrease with the increasing fibre length; the maximum output power occurs at a fibre length of ∼5 m. It also can be seen that the maximum output laser powers for different R_2 are different, which shows that the reflectance of LR FBG strongly affects the laser performance. Figure 8 shows the calculated absorption rate of pump power versus the fibre length for a launched pump power of 20 W. Comparing with Fig. 7, we observe that the maximum output power does not occur at the highest absorption rate but occurs at 83% of the highest absorption rate, which is due to the high propagation loss coefficient of the fibre.

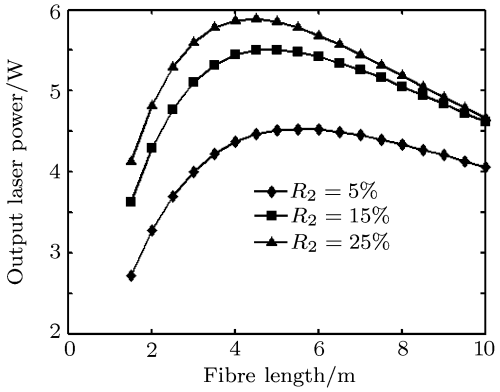


Fig. 7. Calculated output laser power versus fibre length for R_2 of 5%, 15% and 25%, respectively, where the launched pump power is 20 W.

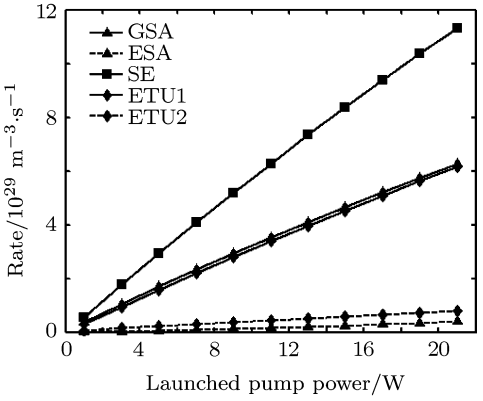


Fig. 6. Transition rates of GSA, ESA, SE, ETU_1 and ETU_2 at fibre front end versus launched pump power.

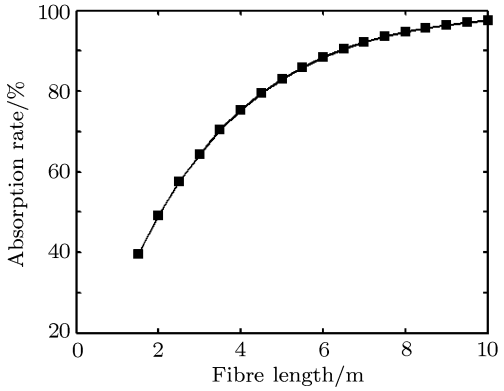


Fig. 8. Calculated absorption rate of pump power versus fibre length for the launched pump power of 20 W.

Figure 9 shows the variation of output laser power versus R_2, where the launched pump power is set at 20 W and the fibre length is set to the optimised value of 5 m. It can be seen that the output laser power first increases and then decreases with the increasing R_2, and attains the maximum value of 5.89 W at $R_2 = 30\%$. This maximum output laser power is $\sim$1 W higher than the experimental result in Ref. [13] for a pump power of 20 W. To show further the difference of the optimised and the experimental results, the calculated output laser power versus the launched pump power using the optimised parameters ($R_2 = 30\%$, $L = 5$ m) and experimental parameters ($R_2 = 15\%$, $L = 6.6$ m) are shown in Fig. 10. It is observed that the slope efficiency with optimised parameters is $\sim 4\%$ higher than that with experimental parameters.

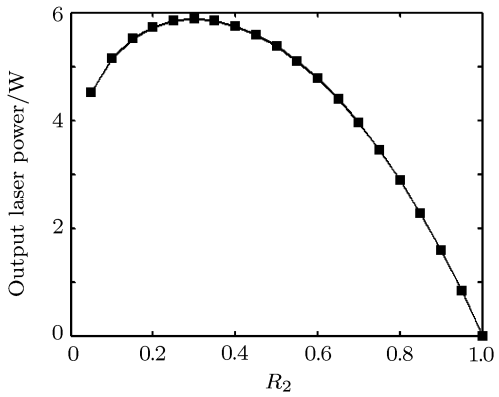


Fig. 9. Variation of output laser power versus R_2, where the launched pump power is 20 W and the fibre length is 5 m.

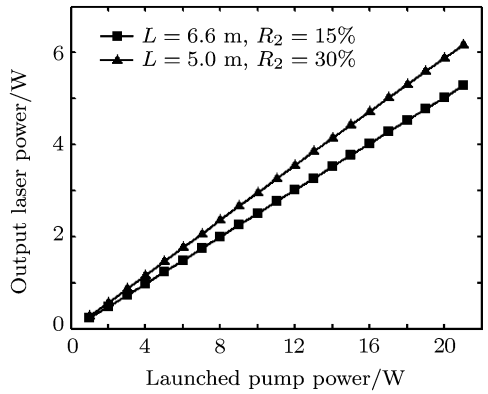


Fig. 10. Calculated output laser power versus launched pump power with the optimised parameters ($R_2 = 30\%$, $L = 5$ m) and with the experimental parameters ($R_2 = 15$ %, $L = 6.6$ m).

Then, we investigate the effect of pumping configurations on the laser performance. Figure 11 shows the calculated output laser power versus launched pump power for forward, backward and two-end pumping (half pump power at each side), respectively, where the fibre length and R_2 are set to be 5 m and 30%, respectively. It is observed that the differences of slope efficiency among above three pumping configurations are very small. The slope efficiency for forward pumping is calculated to be 29.2%, which is only 0.09% and 0.53% higher than that for two-end pumping and backward pumping, respectively. Although the slope efficiency for forward pumping is the highest, the two-end pumping configuration is suggested since it can evenly distribute the heat along the fibre and decrease the maximum temperature at the fibre end.

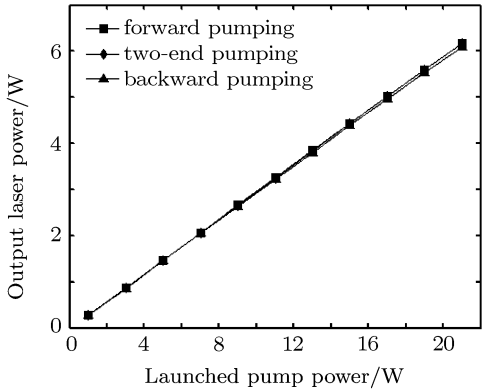


Fig. 11. Calculated output laser power versus launched pump power for forward, backward and two-end pumping configuration, respectively, where the fibre length is 5 m and R_2 is 30%.

4. Conclusion

Based on the rate equations describing the single erbium-doped ZBLAN fibre laser with different pumping configurations being taken into account, we have investigated the population mechanism and the operation performance of the all-fibre erbium-doped ZBLAN double-clad fibre laser demonstrated in Ref. [13]. It is shown that the GSA, ESA, SE and ETU processes can co-exist and construct a population balance, making the laser operate at a stable CW state. The calculation results also show a good agreement with the experimental measurements. In addition, we theoretically optimise the laser structure parameters including fibre length, reflectance of output FBG and pumping configurations. By using the optimised results, the laser slope efficiency can be improved. We expect a high slope efficiency all-fibre mid-IR erbium ZBLAN fibre laser with output powers exceeding 20 W at 2.94 μm can be obtained in the near future.

References

[1] Frenz M, Pratisto H, Konz F, Jansen E D, Welch A J and Weber H P 1996 *IEEE J. Quantum Electron.* **32** 2025

[2] Jackson S D and Lauto A 2002 *Lasers Surg. Med.* **30** 184

[3] Raghunathan V, Borlaug D, Rice R R and Jalali B 2007 *Opt. Express* **15** 14355

[4] Tittle F, Richter D and Fried A 2003 *Top. Appl. Phys.* **89** 445

[5] Wesendahl T, Janknecht P Ott B and Frenz M 2000 *Invest. Ophtalmol. Vis. Sci.* **41** 505

[6] Bernier M, Faucher D, Caron N and Vallée R Centre 2009 *Opt. Express* **17** 16941

[7] Tokita S, Murakami M, Shimizu S, Hashida M and Sakabe S 2009 *Opt. Lett.* **34** 3062

[8] Jackson S D 2009 *Opt. Lett.* **34** 2327

[9] Jackson S D 2004 *Opt. Lett.* **29** 334

[10] Tsang Y H, Taher A E El, King T A and Jackson S D 2006 *Opt. Lett.* **14** 678

[11] Jackson S D, King T A and Pollnau M 1999 *Opt. Lett.* **24** 1133

[12] Zhu X S and Jain R 2007 *Opt. Lett.* **32** 26

[13] Faucher D, Bernier M, Caron N and Vallée R Centre 2009 *Opt. Lett.* **34** 3313

[14] Pollnau M and Jackson S D 2001 *IEEE J. Select. Topics Quantum Electron.* **7** 30

[15] Pollnau M and Jackson S D 2002 I*EEE J. Quantum Electron.* **38** 162

[16] Pollnau M, Spring R, Ghisler Ch, Wittwer S, Lüthy W and Weber H P 1996 *IEEE J. Quantum Electron.* **32** 657

[17] Pollnau M 1997 *IEEE J. Quantum Electron.* **33** 1982

[18] Quimby R S, Miniscalco W J and Thompson B 1991 *SPIE* **1581** 72

[19] Wyss Ch, Lüthy W, Weber H P, Rogin P and Hulliger J 1997 *Opt. Commun.* **139** 215